Aalborg Universitet

Dual-Band Shared Aperture Reflectarray and Patch Antenna Array for S- and Ka-Bands

Serup, Daniel E.; Pedersen, Gert Frølund; Zhang, Shuai

Communication

Dual-Band Shared Aperture Reflectarray and Patch Antenna Array for S- and Ka-Band

Daniel Edelgaard Serup, Gert Frølund Pedersen, *Senior Member, IEEE*, and Shuai Zhang, *Senior Member, IEEE*

Abstract—In this communication, a dual-band shared aperture antenna is presented. The proposed antenna achieves dual-band operation by housing both a low-frequency patch antenna array and a high-frequency reflectarray in the same aperture area. The two different antenna types are combined into a single antenna product without any significant performance loss. The antenna has a layered structure that allows the low-frequency antenna array to have both a sufficient impedance bandwidth and realized gain. The antenna has a shared aperture since the high-frequency reflectarray has unit elements within the area of the low-frequency patch antenna array. This allows the antenna to achieve a good realized gain in the high-frequency band. The proposed antenna is fabricated and measured. The prototype is designed for S- and Ka-band resulting in a frequency-ratio of 7.37. The shared aperture size is 156 mm × 156 mm × 4.624 mm ($1.82\lambda \times 1.82\lambda \times 0.05\lambda$ at S-band and $13.4\lambda \times 13.4\lambda \times 0.40\lambda$ at Ka-band). Measurements show the impedance bandwidth to be 200 MHz (6%) and 5.1 GHz (20%) and the peak realized gain to be 13.70 dBi and 27.65 dBi at 3.5 GHz and 25.8 GHz, respectively A very good agreement between the simulated and measured results is observed.

Index Terms—Antenna, Patch Antenna Array, Reflectarray, Dual-band, Shared Aperture, S-band, Ka-band, mm-wave, Satellite.

I. INTRODUCTION

Dual-band antennas have a wide variety of advantages and they are a very popular topic within the field of antenna designs. For low-orbit nano-satellite applications, asymmetrical dual-band antennas operating in the S- and Ka-band are desired. The low-frequency mode can be used for low-speed up-link communication and the high-speed high-frequency mode can be used for down-link communication. For such a configuration the antenna requires a high frequency-ratio, a sufficient low-frequency impedance bandwidth, and a good high-frequency realized gain.

Different methods of achieving dual-band functionality are reported in the literature [1]–[7]. However, these methods are not able to achieve the desired performance characteristics. The reflectarray antenna typology is known to provide a high gain and can achieve dual-band functionality in different ways. One way is to have two sets of unit element distributions in the same aperture area [8], [9]. The two sets of unit elements need to share the same antenna area. Therefore, the number of elements in each set needs to be reduced. With a reduced number of elements, the resulting gain is also reduced. In a multi-layer antenna configurations the two sets of unit elements could be separated on two different substrates layers [10]–[13]. But, to have sufficient distances between the unit elements and the ground plane, the high-frequency mode needs to be on the bottom layer and the low-frequency mode needs to be on the top layer. This means that the low-frequency element distribution needs to be transparent to the high-frequency mode. This will greatly increase the antenna complexity and limits the unit element possibilities.

Dual-band reflectarray can also be designed by using dual-band unit elements [14]–[17]. The dual-band unit elements consist of a high-frequency inner part that is surrounded by a low-frequency outer part. This limits the performance of the high-frequency mode because the separation between the high-frequency unit elements will be large since it is determined by the size of low-frequency elements.

The antenna proposed by this communication has a unique design with unique advantages not found in the literature. The antenna has a high frequency-ratio, a sufficient low-frequency impedance bandwidth and gain, while maintaining a good high-frequency gain. All of which are required for the nano-satellite use-case scenario presented at the beginning of the introduction.

II. ANTENNA CONFIGURATION

Fig. 1 shows the simulation model of the proposed antenna. The antenna is a shared aperture dual-band antenna. The antenna achieves dual-band operation by accommodating both a high-frequency reflectarray antenna and a low-frequency patch antenna array within the same aperture area.
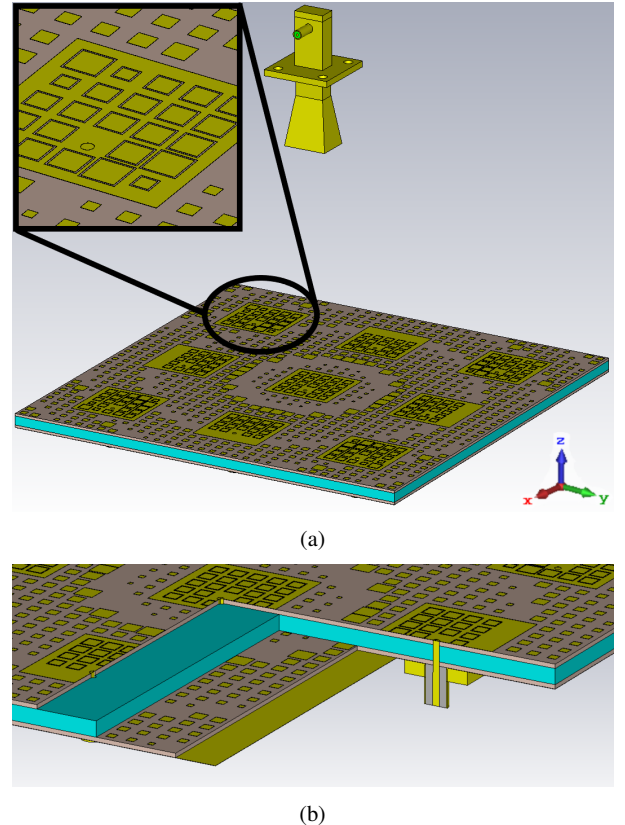

(a)

(b)

Fig. 1: Model of the proposed antenna. (a) Perspective view with a zoomed-in window. (b) Zoomed view of the bottom corner with selected elements cutaway to show the antenna structure.

The square reflective surface of the proposed antenna has a length of 136 mm. The proposed antenna consists of two Rogers RO4003 substrate layers separated by a Polypropylen (PP) layer. Both Rogers RO4003 layers have a thickness of 0.812 mm, a permittivity of 3.55, and a loss tangent of 0.027. The PP layer is 3 mm thick with a permittivity of 2.245 and a loss tangent of 0.002. The bottom of the antenna has a full copper ground plane.

Nine low-frequency patch antennas and 980 smaller square patches are printed on the top substrate layer. The bottom substrate layer houses 980 small patches with identical size and placement as those on the top layer. The small square patches on the top and bottom layers form stacked square patch unit elements as one type of unit cells for the high-frequency reflectarray. Furthermore, 200 square annular loop cuts are made on the nine low-frequency patch antenna elements to form annular square loop unit elements as another type of unit cells for the high-frequency reflectarray. These stacked square patch and annular square loop unit elements generate the desired phase distribution for the high-frequency reflectarray.

The high-frequency reflective surface is fed by a standard gain horn antenna (Pasternack pe9851/2f-10) [18]. This feed is chosen based on its availability to the author. At 25.8 GHz the -3 dBi and -10 dBi beamwidth of the horn antenna is 60° and 108°, respectively. The feed height was optimized through trial-and-error to achieve the highest possible boresight realized gain. A feed height of 80 mm was found to yield the best performance. At 25.8 GHz, this height results in an edge taper of -6.3 dBi.

The low-frequency patch antenna array uses square patch antennas with a length of 22.60 mm. The patch antennas are fed with nine SMA connectors. The connectors are placed 5 mm away from each patch center. The patch antennas have a center-to-center separation of 44 mm in both the X and Y-direction. This distance is equivalent to 0.50λ at 3.5 GHz and 3.78λ at 25.8 GHz.

For this work, all nine elements of the low-frequency 3x3 patch antenna array are excited with identical phase. But, since the antenna elements have independent ports, beamforming could be achieved by exciting different elements with different phase shifts.

III. DESIGN CONSIDERATIONS

The design of the proposed antenna is split into two parts. The first part is to design the low-frequency 3x3 patch antenna array for 3.5 GHz to have sufficient impedance bandwidth and gain. The second part is to design a high-frequency reflectarray with a good realized gain at 25 GHz to 26 GHz.

A. Patch Antenna Array

The impedance bandwidth of the low-frequency antenna is broadened by adding the PP layer. The PP layer increases the distance between the patches and the ground plane which is commonly known to increases the bandwidth of patch antennas. Fig. 2 shows two simulation models. One antenna with a single 0.812 mm RO4003 substrate layer. The other antenna has the proposed configuration of two 0.812 mm RO4003 layers with a 3 mm PP layer between.

Fig 3 shows the simulated S_{11}-parameters of two patch antennas given in Fig. 2. It is seen how the proposed configuration improves the -10 dB impedance bandwidth from 36.0 MHz to 243.4 MHz.

B. Reflectarray Unit Elements

A reflectarray needs a specific unit element phase distribution to transform the spherical waves from the feed into a plane wave in the desired direction. Different phase distributions can be achieved from different types and arrangements of unit elements.
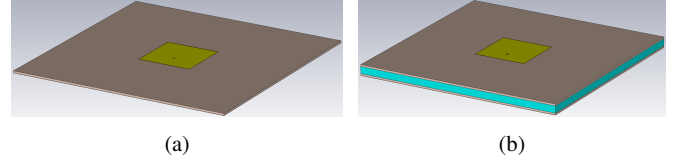

(a)   (b)

Fig. 2: Two patch antenna simulation models. (a) Configuration with a single 0.812 mm RO4003 substrate layer. (b) Configuration with two 0.812 mm RO4003 substrate layers with a 3 mm PP layer between.
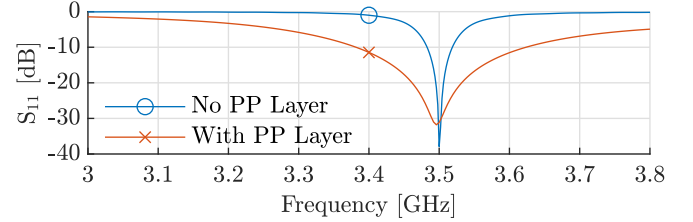

Fig. 3: Simulated S_{11}-parameters of the two antennas seen in Fig. 2.

For the proposed antenna two different unit element types are used. Both elements have a unit cell size of 4 mm. The first element type is a stacked square patch element type and the second element type is the square annular loop element type. The simulation models of the two used unit element types are seen in Fig. 4.
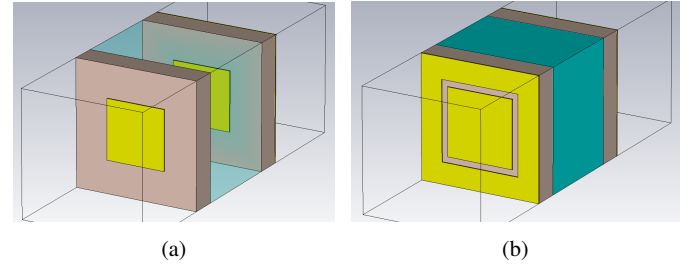

(a)   (b)

Fig. 4: Simulation models of the two used reflectarray unit element types. (a) Stacked square patch unit element type, illustrate with semi-transparent PP layer. (b) Annular square loop unit element type.

These two element types are specifically chosen to match the antenna configuration with two substrate layers separated by a layer of PP material. Fig. 5 shows the relationship between the element size and the resulting phase shifts of the two element types, obtained when considering a perpendicular incident wave. The maximum loss of the patch and the loop type elements is 0.2 and 0.5 dBi, respectively. The stacked square patch type elements are placed around the low-frequency patch antennas while the square annular loop type elements are cut from the actual low-frequency patch antenna elements.
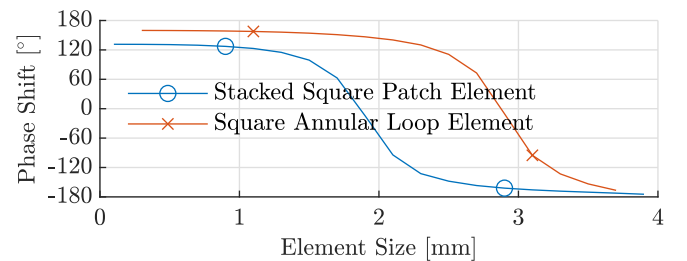

Fig. 5: Simulated phase response of the two used unit element types.

IV. SIMULATION RESULTS

Fig. 6(a) shows the simulated low-frequency radiation pattern constructed by the in-phase combination of the nine low-frequency antenna ports. Fig. 6(b) shows the high-frequency radiation pattern created by the reflectarray part of the antenna. The realized boresight gain of the antenna is 14.92 dBi and 28.84 dBi at 3.5 GHz and 25.8 GHz, respectively.
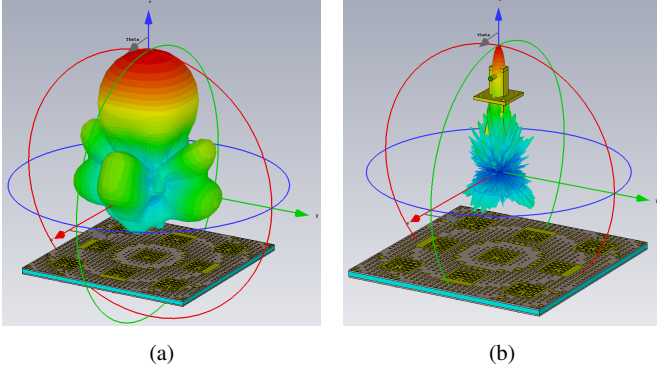

Fig. 6: Simulated radiation pattern of the proposed antenna. Both figures show the realized gain. (a) Low-frequency mode at 3.5 GHz. Created by uniformly combining the nine low-frequency antenna ports. (b) High-frequency mode at 25.8 GHz.

To best evaluate the performance of the proposed antenna, its performance is compared to four other antennas. The four comparison antennas are seen in Fig. 7.
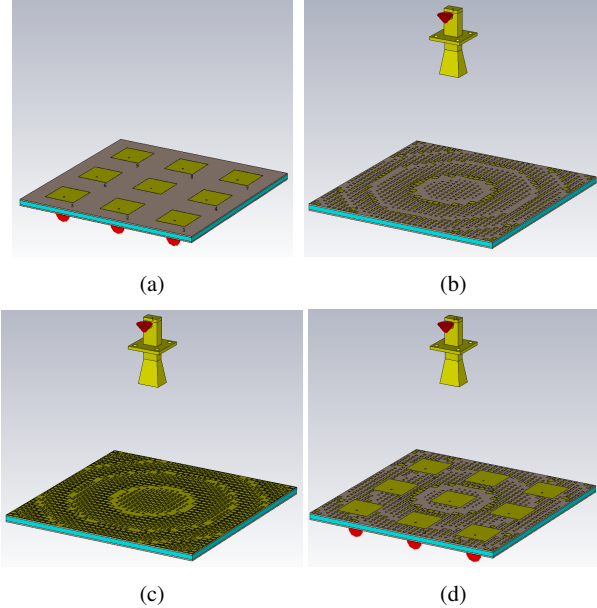

Fig. 7: Simulation models of the four antennas used to evaluate the proposed antenna. (a) A traditional single-band patch antenna array. (b) A single-band reflectarray made purely from stacked square patch elements. (c) A single-band reflectarray made purely from annular loop elements. (d) The proposed antenna without the use of annular loop elements.

First, the low-frequency part of the proposed antenna is compared to the antenna seen in Fig. 7(a). This is a traditional single-band patch antenna array with the same layer plan. The result of the comparison is presented in Fig. 8. The comparison shows that the proposed dual-band antenna matches the performance of the traditional single-band patch antenna array very well. Therefore, it is concluded that the low-frequency part of the proposed antenna is not negatively affected by the high-frequency reflectarray elements and cuts.

Secondly, the high-frequency operation of the proposed antenna is evaluated by comparing it to the three reflectarray antenna configurations given in Fig. 7(b), 7(c), and 7(d). The result of this comparison is provided in Fig. 9. The performance of the proposed antenna is between that of the reflectarray designed purely with patches and the one purely designed with annular loops. In the frequency range from 25 GHz to 26 GHz it is seen that the proposed antenna is comparable to a traditional reflectarray antenna. Additionally, Fig. 9 shows the high-frequency performance improvement achieved by adding the annular cuts on the nine low-frequency patch antennas. Maximum aperture efficiencies for the proposed antenna, the patch only reflectarray, the annular loop only reflectarray, and the proposed antenna without cuts can be calculated as 44.5%, 48.2%, 29.3%, and 24%, respectively.
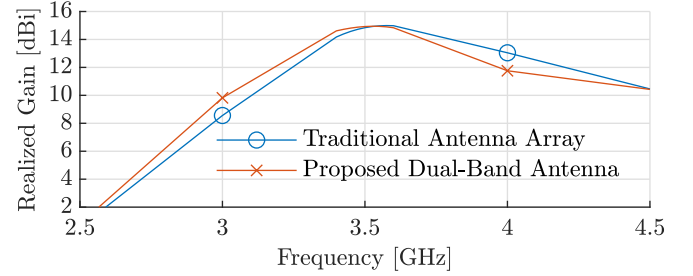

Fig. 8: Simulated performance of the proposed antenna compared to a traditional single-band patch antenna array. The curves are the realized gain of the combined radiation pattern in the boresight direction.
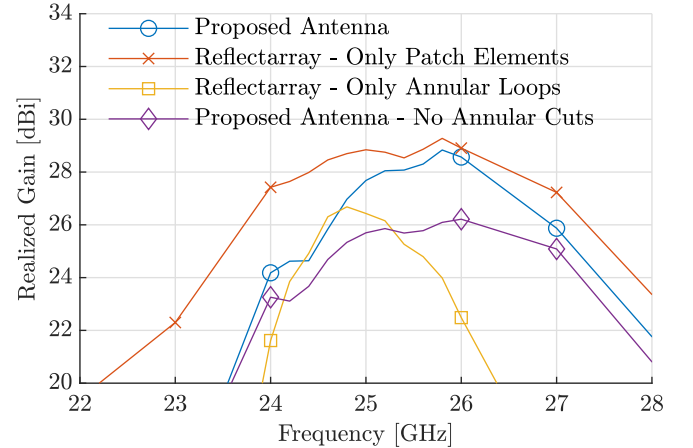

Fig. 9: Simulated performance of the proposed antenna compared to the three other antenna configurations seen in Fig. 7(b), 7(c), and 7(d).

V. MEASUREMENT OF THE ANTENNA PROTOTYPE

To construct an antenna prototype all four edges of the three layers are enlarged by 10 mm. This is done to accommodate screws to keep the three antenna layers together. Additionally, a 3D printed fixture to hold the feed horn is mounted to one side of the board. The fixture is printed with PLA material (Polylactic acid or polylactide). The results of the measurement campaign are compared to an updated simulation model, that includes the feed fixture and the other mentioned minor modifications. Fig. 10 shows the updated simulation model and three pictures of the fabricated antenna prototype.
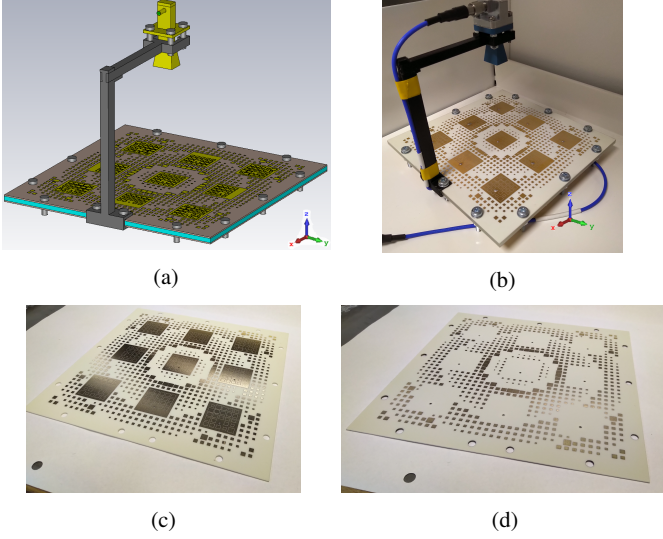

Fig. 10: The antenna prototype. (a) Simulation model. (b) Fully assembled prototype. (c) Top layer. (d) Bottom layer.

The S-Parameters of the antenna are measured with a network analyzer. The nine low-frequency antenna ports are measured individually in a Satimo chamber. Using MatLab, a combined low-frequency radiation pattern is computed as the in-phase superposition of the nine individually measured radiation patterns. The high-frequency radiation pattern is measured in a Mini CATR chamber.

A. Low-Frequency Measurement Results

Fig. 11 shows the measured S-parameters of the low-frequency ports of the prototype antenna. It is seen that all antenna ports have a -10 dB impedance bandwidth of more than 200 MHz. Additionally, the strongest mutual coupling (S-54) is below -16 dB.
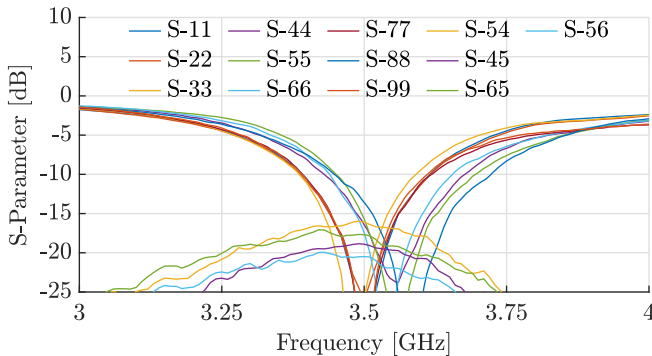

Fig. 11: The measured S-parameters of the nine low-frequency ports of the prototype antenna.

Fig. 12 shows the measured combined radiation pattern of the low-frequency antenna part of the prototype antenna. It is seen that the antenna has a realized gain of 13.70 dBi in the boresight direction, which equals an average array element gain of 4.15 dBi. The low unit element gain is caused by the chosen array configuration. The radiation patterns of the individual array elements are being affected by both the larger ground plane and the surface waves in the substrate. Fig. 13 provides a comparison between the simulated and measured radiation patterns of the prototype antenna in the two orthogonal slices (phi = 0° and phi = 90°). The comparison shows that the radiation pattern of the prototype antenna is symmetrical and that the measured performance matches the simulated. Please note that the measured cross-polarization levels are not given as they are at least 23 dB lower than the co-polarization ones.
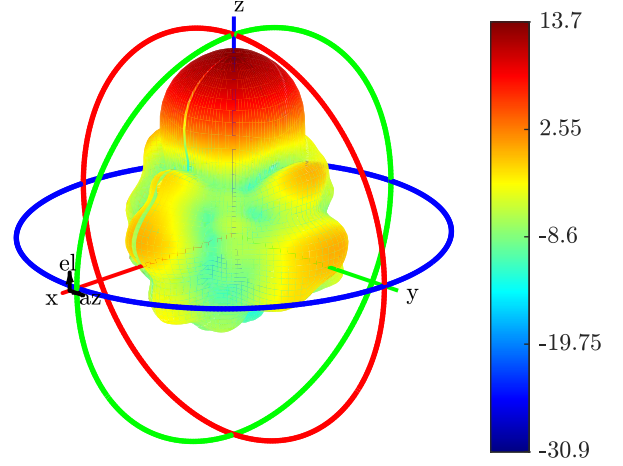

Fig. 12: The combined radiation pattern of the antenna prototype at 3.5 GHz. Computed as the in-phase superposition of the nine individually measured radiation patterns. The figure shows the realized gain.
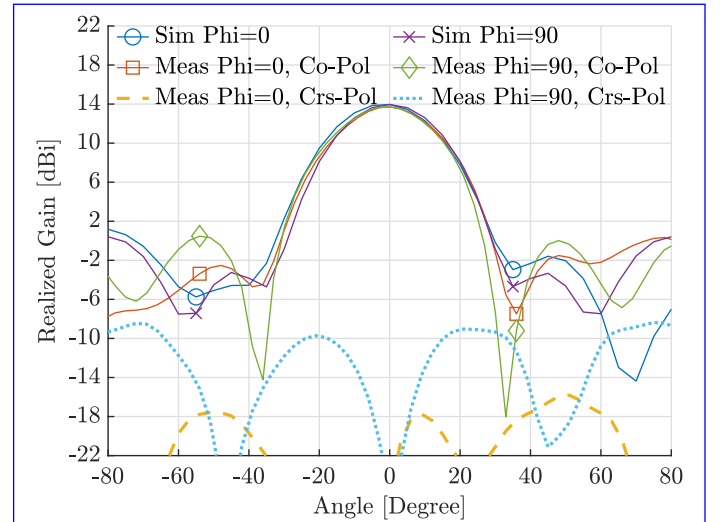

Fig. 13: Simulated and measured radiation pattern slices. All curves represent the realized gain at 3.5 GHz.

Fig. 14 shows a comparison between the simulated and measured realized gain of the prototype antenna in the boresight direction. It is observed that the measured results are in good agreement with the simulated.
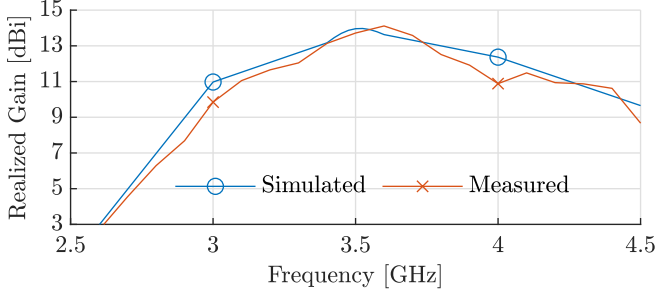

Fig. 14: Simulated and measured realized gain of the prototype antenna in the boresight direction.

B. High-Frequency Measurement Results

Figure 15 shows the measured S_{11} of the antenna prototype as well as the feed horn alone. The -10 dB impedance bandwidth of the high-frequency part of the prototype antenna is measured to be 5.1 GHz, from 23.25 GHz to 28.35 GHz.
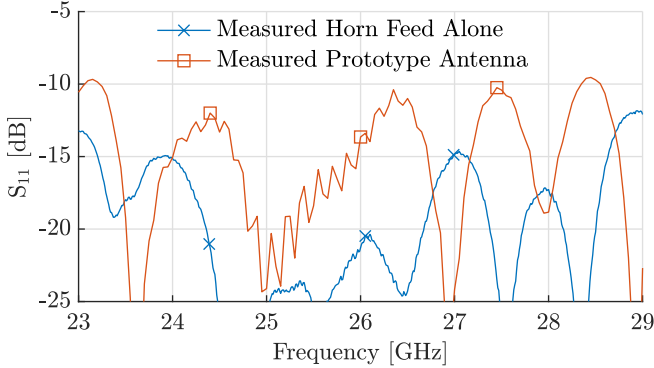

Fig. 15: Measured S_{11}-parameter of the antenna prototype compared to the feed horn alone.

Fig. 16 shows the measured high-frequency radiation pattern of the antenna prototype, where the realized gain is 27.65 dBi at 25.8 GHz. Fig. 17 presents a comparison between the simulated and measured radiation patterns in the two orthogonal slices (phi = 0° and phi = 90°). A good agreement between the simulated and measured main beam radiation pattern is observed. However, it is noted that the side lobe levels are measured relatively lower than indicated by the simulation. The plot does not show the cross-polarization levels, as the measured cross-polarization level is at least 23 dB lower than the co-polarization. Fig. 18 gives a comparison between the simulated and measured realized gain of the high-frequency antenna in the boresight direction. A good agreement between the simulated and the measured gain characteristics is observed. In addition, Fig. 18 shows that the beamwidth of the antenna is greater than 4° in the full high-frequency band.

When comparing the simulated antenna gains in Section IV to the gain presented in Section V a gain difference of 1.2 dBi can be observed for the two center frequencies of 3.5 GHz and 25.8 GHz. This gain difference is caused by the mounting fixture for the feeding horn antenna.
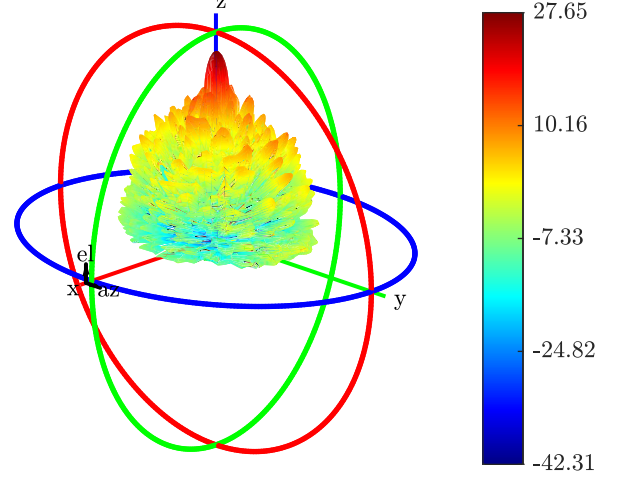

Fig. 16: The measured radiation pattern of the antenna prototype at 25.8 GHz. The figure shows the realized gain.
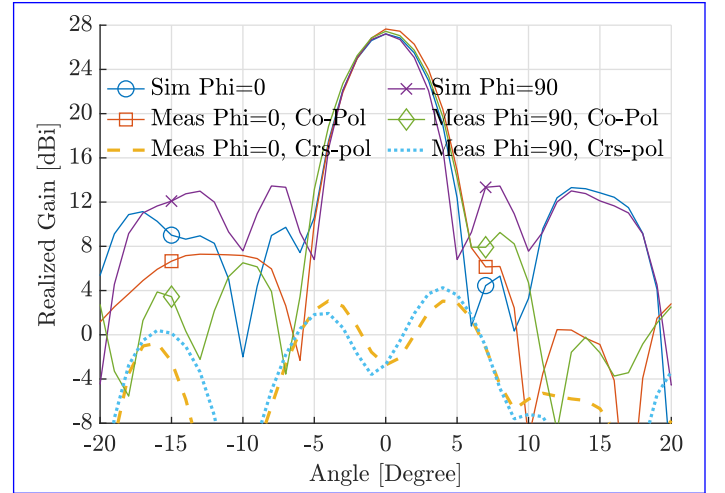

Fig. 17: Simulated and measured radiation pattern slices. All curves represents the realized gain at 25.8 GHz.
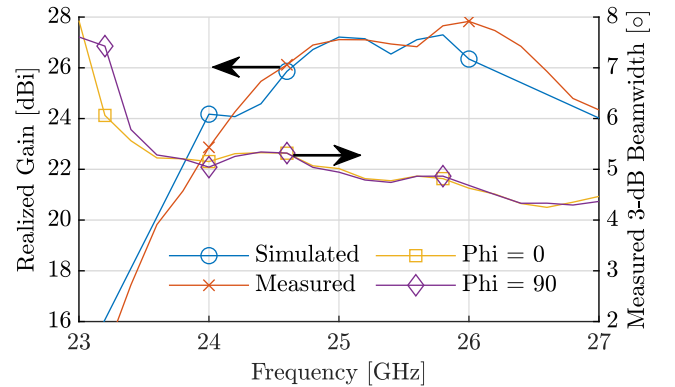

Fig. 18: (Left) Simulated and measured realized gain of the prototype antenna in the boresight direction. (Right) Measure 3 dB beamwidth of the prototype antenna.

C. Comparison with the State-of-Art

Tab. I provides a performance comparison between the proposed antenna and other antennas from the literature. It is found that the proposed antenna achieves a high frequency-ratio and has a very compact size compared with the ones in the state-of-art. The proposed antenna has a sufficient low-frequency impedance bandwidth and realized gain. Moreover, the comparison shows that despite its compact size and good low-frequency performance the designed antenna still manages to simultaneously maintain a good high-frequency realized gain. From the comparison, it is clear that the unique design of the proposed antenna allows it to achieve the performance characteristics required for the nano-satellite use-case presented in the introduction.

TABLE I: Performance comparison between the proposed antenna and other antennas found in the state-of-the-art literature.

Performance Metric	This Work	[1]	[2]	[3]	[14]
Center Frequency [GHz]	3.5 & 25.8	3.6 & 25.8	3.6 & 28	5.3 & 9.6	9.7 & 19.2
Frequency Ratio	7.37	7.16	7.78	1.81	1.98
Impedance bandwidth [%]	6 & 20	23.5 & 4.8	-	-	-
Surface Size [mm]	136x136	93x93	92x92	140x140	300 Circular
Surface Size [λ]	1.59 & 11.70	1.12 & 8.00	1.10 & 8.59	2.47 & 4.48	9.70 & 19.2
Surface Height [mm]	4.624	6.9	7.34	31	2.313
Realized Gain [dBi]	13.7 & 27.65	10.9 & 22.4	10.0 & 14.0	16.0 & 20.0	
Aperture Efficiency [%]	74 & 34	65 & 34	65 & 3	13 & 40	63 & 42

VI. Conclusion

A shared aperture dual-band reflectarray and patch antenna array for S- and Ka-band have successfully been designed. The proposed antenna achieves dual-band operation by housing both a S-band patch antenna array and a Ka-band reflectarray in the same aperture area.

A prototype has been fabricated and measured. From the measured results, the antenna prototype achieves a $-10\,\mathrm{dB}$ impedance bandwidth of $200\,\mathrm{MHz}$ and a peak gain of $13.70\,\mathrm{dBi}$ at the lower center frequency of $3.5\,\mathrm{GHz}$. The measurement confirms that the prototype antenna has a realized gain of $27.65\,\mathrm{dBi}$ at a frequency of $25.8\,\mathrm{GHz}$, resulting in an aperture efficiency of $34\,\%$. The measured antenna performance aligns very well with the simulations. Therefore, it is concluded that this method of achieving high frequency-ratio dual-band operation in a shared aperture is very convenient and yields good performance.

REFERENCES

[1] T. Li and Z. N. Chen, "Metasurface-Based Shared-Aperture 5G S -/ K -Band Antenna Using Characteristic Mode Analysis," *IEEE Trans. Antennas Propag.*, vol. 66, no. 12, pp. 6742-6750, Dec. 2018.

[2] T. Li and Z. N. Chen, "Shared-Surface Dual-Band Antenna for 5G Applications," *IEEE Trans. Antennas Propag.*, vol. 68, no. 2, pp. 1128-1133, Feb. 2020.

[3] F. Qin et al., "A Simple Low-Cost Shared-Aperture Dual-Band Dual-Polarized High-Gain Antenna for Synthetic Aperture Radars," *IEEE Trans. Antennas Propag.*, vol. 64, no. 7, pp. 2914-2922, July 2016.

[4] L. Guo, P. Tan and T. Chio, "Single-Layered Broadband Dual-Band Reflectarray With Linear Orthogonal Polarizations," *IEEE Trans. Antennas Propag.*, vol. 64, no. 9, pp. 4064-4068, Sept. 2016.

[5] T. Smith, U. Gothelf, O. S. Kim and O. Breinbjerg, "An FSS-Backed 20/30 GHz Circularly Polarized Reflectarray for a Shared Aperture L- and Ka-Band Satellite Communication Antenna," *IEEE Trans. Antennas Propag.*, vol. 62, no. 2, pp. 661-668, Feb. 2014.

[6] C. Mao, S. Gao, Y. Wang, Q. Chu and X. Yang, "Dual-Band Circularly Polarized Shared-Aperture Array for C -/ X -Band Satellite Communications," *IEEE Trans. Antennas Propag.*, vol. 65, no. 10, pp. 5171-5178, Oct. 2017.

[7] A. I. Sandhu, E. Arnieri, G. Amendola, L. Boccia, E. Meniconi and V. Ziegler, "Radiating Elements for Shared Aperture Tx/Rx Phased Arrays at K/Ka Band," *IEEE Trans. Antennas Propag.*, vol. 64, no. 6, pp. 2270-2282, June 2016.

[8] Y. Chen, L. Chen, H. Wang, X. Gu and X. Shi, "Dual-Band Crossed-Dipole Reflectarray With Dual-Band Frequency Selective Surface," *IEEE Antennas Wireless Propag. Lett.* vol. 12, pp. 1157-1160, 2013.

[9] J. Zhao et al., "A Low-Mutual Coupling Dual-Band Dual-Reflectarray Antenna With the Potentiality of Arbitrary Polarizations," *IEEE Antennas Wireless Propag. Lett.* vol. 16, pp. 3224-3227, 2017.

[10] C. Han, J. Huang and Kai Chang, "A high efficiency offset-fed X/ka-dual-band reflectarray using thin membranes," *IEEE Trans. Antennas Propag.*, vol. 53, no. 9, pp. 2792-2798, Sept. 2005.

[11] M. R. Chaharmir and J. Shaker, "Design of a Multilayer X-/Ka-Band Frequency-Selective Surface-Backed Reflectarray for Satellite Applications," *IEEE Trans. Antennas Propag.*, vol. 63, no. 4, pp. 1255-1262, April 2015.

[12] R. Deng, F. Yang, S. Xu and M. Li, "An FSS-Backed 20/30-GHz Dual-Band Circularly Polarized Reflectarray With Suppressed Mutual Coupling and Enhanced Performance," *IEEE Trans. Antennas Propag.*, vol. 65, no. 2, pp. 926-931, Feb. 2017.

[13] D. Martinez-de-Rioja, R. Florencio, E. Martinez-de-Rioja, M. Arrebola, J. A. Encinar and R. R. Boix, "Dual-Band Reflectarray to Generate Two Spaced Beams in Orthogonal Circular Polarization by Variable Rotation Technique," *IEEE Trans. Antennas Propag.*, vol. 68, no. 6, pp. 4617-4626, June 2020.

[14] R. Shamsaee Malfajani and B. Abbasi Arand, "Dual-Band Orthogonally Polarized Single-Layer Reflectarray Antenna," *IEEE Trans. Antennas Propag.*, vol. 65, no. 11, pp. 6145-6150, Nov. 2017.

[15] X. Li, X. Li and L. Yang, "Single-Layer Dual-Band Wide Band-Ratio Reflectarray With Orthogonal Linear Polarization," *IEEE Access,* vol. 8, pp. 93586-93593, 2020.

[16] S. Qu, Q. Chen, M. Xia and X. Y. Zhang, "Single-Layer Dual-Band Reflectarray With Single Linear Polarization," *IEEE Trans. Antennas Propag.*, vol. 62, no. 1, pp. 199-205, Jan. 2014.

[17] R. Deng, Y. Mao, S. Xu and F. Yang, "A Single-Layer Dual-Band Circularly Polarized Reflectarray With High Aperture Efficiency," *IEEE Trans. Antennas Propag.*, vol. 63, no. 7, pp. 3317-3320, July 2015.

[18] WR-34 Waveguide Standard Gain Horn Antenna (PE9851/2F-10) by Pasternack Enterprises Inc. Available at: https://www.pasternack.com/standard-gain-horn-waveguide-size-wr34-10-db-gain-292mm-female-pe98512f-10-p.aspx